Dissolution in a field

W. Hwang* and S. Redner
Center for BioDynamics, Center for Polymer Studies, and Department of Physics, Boston University, Boston, Massachusetts 02215
(Received 1 June 2001; published 26 September 2001)

We study the dissolution of a solid by continuous injection of reactive ''acid'' particles at a single point, with the reactive particles undergoing biased diffusion in the dissolved region. When acid encounters the substrate material, both an acid particle and a unit of the material disappear. We find that the lengths of the dissolved cavity parallel and perpendicular to the bias grow as $t^{2/(d+1)}$ and $t^{1/(d+1)}$, respectively, in d dimensions, while the number of reactive particles within the cavity grows as $t^{2/(d+1)}$. We also obtain the exact density profile of the reactive particles and the relation between this profile and the motion of the dissolution boundary. The extension to variable acid strength is also discussed.

DOI: 10.1103/PhysRevE.64.041606 PACS number(s): 68.43.−h, 47.70.−n, 44.35.+c, 05.40.Jc

I. INTRODUCTION

The dissolution of a solid material by contact with a reactive fluid is a fundamental process that underlies corrosion [1], diagenesis [2,3], erosion [4], etching [5,6], and many other industrial processes. The same dynamical process can also be viewed as the melting of a solid by heating the material at a single point in the interior [7]. These types of dissolution (or melting) processes are described by the motion of the interface between the reactive fluid and the solid. In many situations, molecular diffusion is the transport mechanism for the reactive particles, and this leads to diffusion-controlled moving boundary-value problems [8,9].

In this paper, we consider the kinetics of this dissolution process when there is a superimposed bias on the diffusive motion of the acid. Such a bias can be easily realized, for example, by an electric field acting on ionized particles, or by a gravitational field or a pressure gradient acting on a flowing fluid. We find that the bias is a relevant perturbation with respect to molecular diffusion and gives rise to a dissolution process different from that caused by isotropic diffusion [10]. As a function of time, the size of the dissolved region grows continuously and preferentially in the direction of the bias (Fig. 1). The basic questions that we shall study are the density profile of the acid particles inside the dissolved cavity, as well as the shape and time dependence of the boundary between the fluid and unreacted material.

In Sec. II, we first define the model and write the reaction diffusion equation that governs the density of reactive particles in the continuum limit. In Sec. III, we then solve for the steady-state density profile of reactive particles in the dissolved cavity. This profile satisfies the anisotropic Laplace equation, which is the time-independent limit of the basic equation of motion. In Sec. IV, we investigate the motion of the interface and determine the different characteristic lengths of the cavity in the directions parallel and perpendicular to the bias. We briefly summarize in Sec. V and also discuss a generalization of the system to variable acid strength.

*Present address: Center for Biomedical Engineering, Massachusetts Institute of Technology, Cambridge, MA 02139.

II. THE MODEL

We consider the following microscopic dissolution process (Fig. 1). Initially, all sites are unreacted. Acid particles are injected at rate λ at the origin of a d-dimensional solid substrate. After injection, an acid particle undergoes biased diffusion until it hits a site at the interface between unreacted substrate and the dissolved cavity. In this interaction, both the host substrate site and the acid disappear. We can think of the acid as having unit strength so that one acid particle and one substrate particle are consumed in a reaction. Later, we will generalize to allow acid to dissolve many substrate sites before being neutralized. In the context of melting, we can think of particle injection as the localized input of heat and dissolution as the melting of the solid when heat reaches the interface.

In the limiting case where the reactive particles undergo isotropic diffusion, the resulting dissolution process has been extensively studied, both in the context of melting [7] and in the framework of diffusion-controlled reactions [10]. Here the radius of the dissolved region $R(t)$ grows as $(t \ln t)^{1/2}$ and as $t^{1/d}$ for spatial dimension $d=1$ and $d \geqslant 2$, respectively. The density profile of the acid particles is also radially symmetric and asymptotically approaches a steady state as a function of the scaled radial distance $r/R(t)$.

These results have a simple origin. In $d=1$, for N diffusing particles initially located at the origin, the furthest particle from the origin after time t will be a distance of the order of $(t \ln N)1/2$ [11]. Thus, if λt acid particles are injected continuously at the origin, the most distant particle,

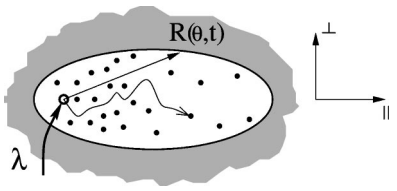

FIG. 1. Schematic illustration of the dissolution process. Reactive particles (dots) are continuously injected at rate λ at a single point (circle). Each particle undergoes biased diffusion, with bias in the parallel direction. When a particle reaches the boundary of the dissolved cavity, a unit of the host material and the particle both disappear.

and therefore, the position of the interface should be $(t \ln \lambda t)^{1/2}$ from the origin. For $d \geqslant 2$, since each acid particle dissolves a single substrate particle, the dissolved volume can be at most λt. Consequently, the radius can be no larger than $t^{1/d}$ for $d \geqslant 2$. Within the dissolved cavity, the density profile of acid particles away from the interface approaches a static limit for $d>2$. This density profile thus obeys the Laplace equation and decays as r^{2-d}. For $d \leqslant 2$, the density profile is not static and it can be obtained conveniently by a scaling solution [10].

In the presence of the bias, we need to consider separately the growth parallel and perpendicular to the bias. The dynamics of this anisotropic dissolution process is governed by $c(\vec{r},t)$, the concentration of acid at position $\vec{r}$ within the dissolved region at time t. This concentration obeys the convection-diffusion equation

$$\frac{\partial c}{\partial t} + v \frac{\partial c}{\partial x} = D \nabla^2 c + \lambda \delta(\vec{r}), \tag{1}$$

subject to the absorbing boundary condition $c(\vec{r},t)=0$ for $|\vec{r}|=R(\theta,t)$, where $R(\theta,t)$ is the radius of the moving interface as a function of θ and t (Fig. 1). Here, we have taken the bias direction as along x. The motion of the interface is then governed by the flux of acid onto the interface

$$\frac{\partial \vec{R}}{\partial t} = -KD \vec{\nabla} c\big|_{|\vec{r}|=R(\theta,t)}, \tag{2}$$

where K is the parameter that quantifies the acid strength. Here, we define this constant to be one and later generalize to arbitrary acidity. Notice, also, that there is no convective contribution to this flux (vc) because of the absorbing boundary condition.

A basic feature that simplifies much of the analysis is that the density profile of the acid within the dissolved region is stationary in time except near the boundary. This arises because the input of particles compensates for their loss at the boundary. This same simplifying feature, which also applies in the case of isotropic diffusion for $d>2$, ultimately stems from the transient nature of biased diffusion [12]. We now exploit this stationarity to obtain the exact concentration profile of acid within the dissolved cavity.

III. STEADY-STATE CONCENTRATION PROFILE

Setting the time derivative in Eq. (1) equal to zero, an anisotropic Laplace equation results. For zero bias, this gives the classical Laplace equation with steady-state solution $c_{ss}(\vec{r}) \propto r^{2-d}$ for $d>2$. To find the corresponding solution in the presence of a bias, we perform a Fourier transform of the anisotropic Laplace equation to yield

$$-D\vec{k}^2 \tilde{c}(\vec{k}) + iv k_x \tilde{c}(\vec{k}) + \lambda = 0, \tag{3}$$

with solution

$$\tilde{c}(\vec{k}) = \frac{\lambda}{D\vec{k}^2 - iv k_x}. \tag{4}$$

Inverting this Fourier transform gives the steady-state acid concentration

$$\begin{aligned} c_{ss}(\vec{r}) &= \int \frac{d\vec{k}}{(2\pi)^d} \tilde{c}(\vec{k}) e^{-i\vec{k}\cdot\vec{r}} \\ &= \frac{\lambda}{(2\pi)^d D} \int d\vec{k} \, \frac{e^{-i\vec{k}\cdot\vec{r}}}{\vec{k}^2 - iv k_x/D} \\ &= \frac{\lambda}{(2\pi)^d D} \int d\vec{k} \, \frac{e^{-i\vec{k}\cdot\vec{r} + vx/2D}}{k^2 + (\vec{v}2/D)^2}. \end{aligned} \tag{5}$$

In the last step, we complete the square in the denominator and then shift k_x by $k_x - iv/2D$. The last integral in Eq. (5) is [13],

$$c_{ss}(\vec{r}) = \frac{\lambda e^{vx/2D}}{(2\pi D)^{d/2}} \left(\frac{v}{2r}\right)^{d/2-1} K_{d/2-1}\left(\frac{vr}{2D}\right), \tag{6}$$

where $K_{d/2-1}$ is the modified Bessel function.

This exact solution has very different forms in the regions $x>0$ and $x<0$. In the interesting case of $x \gg 0$, we substitute the asymptotic expansion $K_\nu(z) \sim (\pi/2z)^{1/2} e^{-z}$ [14] into Eq. (6) to obtain

$$c_{ss}(\vec{r}) \sim \frac{\lambda}{v} \left(\frac{v}{4\pi D r}\right)^{(d-1)/2} e^{-v(r-x)/2D}. \tag{7}$$

In the special cases of $d=1$, 2, and 3, this reduces to

$$c_{ss}(\vec{r}) = \begin{cases} \dfrac{\lambda}{v}, & d=1 \\ \dfrac{\lambda}{\sqrt{4\pi D v r}} e^{-v(r-x)/2D}, & d=2 \\ \dfrac{\lambda}{4\pi D r} e^{-v(r-x)/2D}, & d=3. \end{cases} \tag{8}$$

Conversely, for $x<0$, $c_{ss}(\vec{r})$ decays exponentially as a function of the distance from the origin, with the length scale of this decay proportional to D/v.

IV. INTERFACE MOTION

To gain a fuller appreciation for time-dependent features and the motion of the interface, we have performed Monte Carlo simulations of the dissolution process. Our simulations are based on simply tracking the motion of all the reactive-particles. Each particle performs a biased nearest-neighbor random walk on a d-dimensional hypercubic lattice, with hopping probability equal to $1/(2d)$ in the $2d-2$ directions perpendicular to the bias, and equal to $1/(2d) < p_+ < 1/d$ and $p_- = 1/d - p_+ < p_+$ in the $\pm x$ directions, respectively. These hopping probabilities give a bias velocity $v = p_+ - p_-$, as

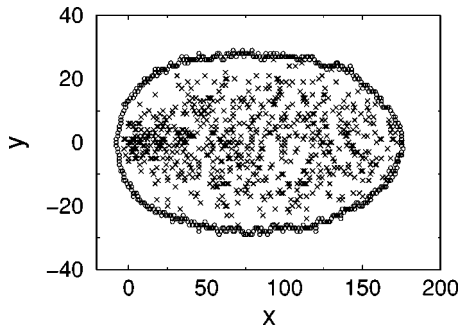

FIG. 2. Typical shape of the dissolved region on the square lattice after $t=10^4$ time steps. Reactive particles and sites on the dissolution boundary are denoted by crosses and circles, respectively. The injection point is at $(x,y)=(0,0)$ and the bias velocity is $v=0.2$. For this velocity, $vt \gg \sqrt{2Dt}$, and thus, the system is far beyond the initial transient regime.

well as a superimposed isotropic diffusion process, with the diffusion coefficient in all coordinate directions equal to $1/2d$. Henceforth, we fix the injection rate to be $\lambda=1$. Each lattice site is initially regarded as one unit of solid material that disappears when it is contacted by a reactive particle.

The choice of the bias in our simulations is dictated by basic physical considerations. If the bias velocity is too small, there is a long crossover time before the bias dominates over the diffusion. On the other hand, for a bias velocity that is close to the maximum value of $1/d$, the length of the dissolved region becomes extremely large and this requires considerable computer memory to store the data of the system map. For these reasons, we found it optimal to consider intermediate values of the velocity.

As a function of time, an elliptically-shaped dissolved cavity grow in which the interface remains relatively smooth (Fig. 2). This smoothness stems from the same mechanism that lead to preferential tip growth in diffusion-limited aggregation. If there is a protrusion on the surface, it will be preferentially dissolved because of the tendency for a diffusing particle, even in the presence of a bias, to contact such protrusions first. Within this cavity, there is a distribution of mobile reactive particles that have not yet reached the interface. These physical characteristics have different dependences in spatial dimension $d=1$ and in higher dimensions; we therefore discuss these two cases separately.

A. One dimension

We first apply a simple flux balance argument [15] to show that for $x>0$, the interface boundary $R(t)$ moves with a fixed propagation velocity – defined to be v_I – which is less than the particle velocity v. Since the input of reactive-particles occurs at rate λ, the particle flux in the $+x$ direction is simply λ. Thus, a unit flux would lead to an interface velocity v_I/λ. On the other hand, in a reference frame that moves at velocity v, the reactive particles are at rest while the substrate particles (with density ρ) move with velocity $-v$. In this moving frame, a flux of substrate particles $-\rho v$ would lead to the interface moving at velocity v_I-v. Therefore, a unit particle flux would give an interface velocity $(v_I-v)/(-\rho v)$. Since the reaction has the symmetrical stoichiometry $A(\text{acid})+B(\text{substrate})\rightarrow 0$, the two velocities under conditions of unit flux must be equal. This then leads to the interface velocity

$$v_I=\lambda v/(\lambda+\rho v). \tag{9}$$

For $r\approx R$, the density profile decreases sharply from the constant value λ/v [Eq. (8)] to 0. Because the dissolution process is equivalent to the reaction $A+B\rightarrow 0$ with components approaching each other at finite velocity, the width of the reaction front is proportional to D/v and does not grow in time [15,16]. We have also verified these features by Monte Carlo simulation (data not shown).

B. Dimensions $d\geqslant 2$

For $d\geqslant 2$, let us locate the reactive particles by the d-dimensional cylindrical coordinates $\vec{r}=(x,\vec{r}_\perp)$, where $\vec{r}_\perp$ is the $(d-1)$-dimensional radial vector perpendicular to the x axis. Similarly, we write $\vec{R}=(R_\parallel,\vec{R}_\perp)$ to denote the position of the interface. Since the dissolved cavity grows predominantly along the direction of the bias, we focus our attention on this downstream portion of the interface.

We now determine how $R_\parallel$ and $R_\perp$ depend on time. Let us assume that $R_\parallel\sim t^{\nu_\parallel}$ and $R_\perp\sim t^{\nu_\perp}$. Since the motion of the reactive particles in the transverse direction is diffusive, we expect that $R_\perp\propto R_\parallel^{1/2}\sim t^{\nu_\parallel/2}$. Then the volume of the dissolved region is proportional to $V\sim R_\parallel R_\perp^{d-1}\sim t^{(d+1)\nu_\parallel/2}$. Since V cannot grow faster than λt, we must have $(d+1)\nu_\parallel/2\leqslant 1$. On the other hand, if V were to grow slower than λt, the number of reactive particles in the dissolved region would have to grow with time, in contradiction with the steady-state density profile derived above. Thus, V should grow linearly with time, from which we conclude that $\nu_\parallel=2/(d+1)$. Hence,

$$R_\parallel\sim t^{2/(d+1)}, \quad R_\perp\sim t^{1/(d+1)}. \tag{10}$$

These predictions are in very good agreement with our numerical simulations (Fig. 3).

The dependence of $R_\parallel$ on t can also be determined independently from the density profile $c(\vec{r},t)$. Similar to the case of $d=1$, $c(\vec{r},t)$ approaches c_{ss} far from the interface, while $c(\vec{r},t)$ assumes a traveling-wave form near the interface-,which rapidly decays from $c$ss to 0 (Fig. 4). From the inset to this figure, we see that the width of this front does not grow in time. Using Eq. (2), we can then approximate the equation of motion for the interface as $\dot{R}\sim c_{ss}/w$, where $w\sim D/v$ is the width of the front. Substituting the asymptotic expansion for $K_\nu(z)$ in Eq. (6) then gives $c_{ss}(R_\parallel)\sim R_\parallel^{(1-d)/2}$. Using this in $\dot{R}\sim c_{ss}/w$, we obtain $R_\parallel\sim(t/w)2/(d+1)$, in agreement with Eq. (10).

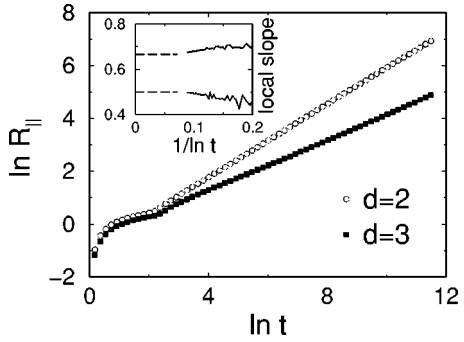

FIG. 3. Plot of $R_\parallel$ versus t on a double logarithmic scale for $d=2$ and 3 (bias velocity $v=0.3$ for both cases). The data represent averages over 500 ($d=2$) and 1000 ($d=3$) realizations and are taken at time 1.2^n with $n \leqslant 63$. The inset shows the local slopes of the data versus $1/\ln t$. These appear to converge to 2/3 in $d=2$ and 1/2 in $d=3$ (dashed lines), in agreement with Eq. (10).

C. Scaling for the density profile

To obtain the number of reactive particles, it is convenient to express their density profile in a scaled form. Based on the time dependences of $R_\parallel$ and $R_\perp$, we introduce the scaled variables $\xi_\parallel = x/t^{2/(d+1)}$ and $\vec{\xi}_\perp = \vec{r}_\perp / t^{1/(d+1)}$. In terms of these scaled coordinates,

$$r=(x^2+\vec{r}_\perp^{\,2})^{1/2} \simeq t^{2/(d+1)}\xi_\parallel + \frac{1}{2}\frac{\xi_\perp^2}{\xi_\parallel}. \tag{11}$$

Using the asymptotic expansion of K_ν, and substituting the scaled variables into Eq. (6), we obtain the scaling form for the density profile

$$\begin{aligned} c(\xi_\parallel, \vec{\xi}_\perp, t) &\sim t^{-(d-1)/(d+1)} \xi_\parallel^{-d/2} \exp\left(-\frac{v}{2D}\frac{\xi_\perp^2}{\xi_\parallel}\right), \\ &\equiv t^{-(d-1)/(d+1)} f(\xi_\parallel, \xi_\perp). \end{aligned} \tag{12}$$

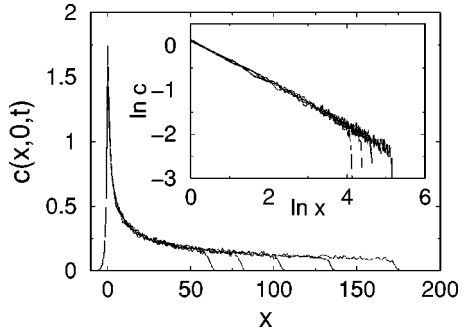

FIG. 4. Density profile of reactive particles in $d=2$ along the x axis at equally spaced times on a logarithmic scale. The bias velocity is $v=0.2$. The data represent averages over 1500 realizations. Inset: same data on a double logarithmic scale. Except for the sharply decreasing interfacial region, the profile $c_{ss}(x,0) \propto x^{-1/2}$ [see Eq. (8)].

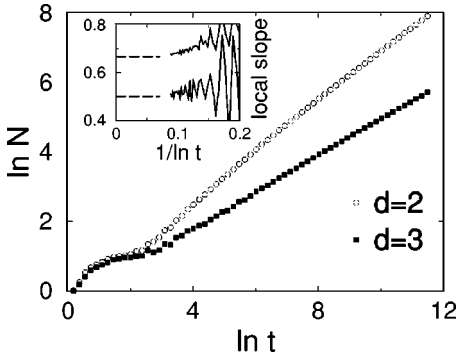

FIG. 5. Plot of $\ln N(t)$ versus $\ln t$. The data are from the same simulations as Fig. 3. The inset shows the local slopes that appear to converge to 2/3 and 1/2 for $d=2$ and 3 (dashed lines), consistent with Eq. (13).

From this form, we easily obtain the time dependence of the total number of active particles $N(t)$ to be

$$\begin{aligned} N(t) &= \int d\vec{r}\, c(\vec{r},t), \\ &\sim t^{2/(d+1)} \int d\xi_\parallel\, d\vec{\xi}_\perp\, f(\xi_\parallel, \vec{\xi}_\perp), \\ &\sim t^{2/(d+1)}. \end{aligned} \tag{13}$$

This prediction is also in excellent agreement with our simulations (Fig. 5).

Alternatively, $N(t)$ equals the difference between the number of injected particles and the volume of the dissolved region. We use this fact to provide a more precise form for the time dependence of the dissolved volume $V(t)$. By multiplying Eq. (2) by the surface element $d\vec{S}$, integrating over the dissolution interface, and using Eq. (1), we have

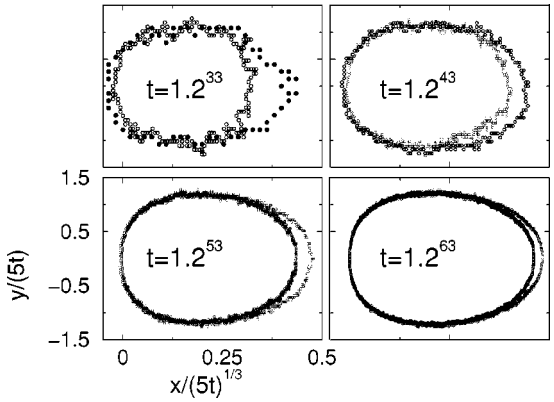

FIG. 6. Scaled boundary profiles for acid strength $A=1$ and $A=5$ at different times. All graphs are on the same scale. The coordinates are divided by $(At)^\nu$, with $\nu=2/3$ for the horizontal scale and $\nu=1/3$ for the vertical scale. The smaller contours are for $A=5$.

$$\int d\vec{S}\cdot\frac{d\vec{R}}{dt} = -D\int d\vec{S}\cdot\vec{\nabla}c|_{\vec{R}}$$
$$= -D\int dV\ \nabla^2 c$$
$$= -\int dV\ [\partial_t c + v\,\partial_x c - \lambda\,\delta(\vec{r})]$$
$$= -\frac{dN}{dt} + \lambda. \tag{14}$$

The left-hand side is simply equal to $\dot{V}$. Therefore, we obtain the obvious conservation equation $(d/dt)(V+N)=\lambda$. Then Eq. (13) gives $V(t)\sim\lambda t-\alpha t^{2/(d+1)}$, where α is a constant related to the integral in Eq. (13).

V. DISCUSSION

In this paper, we studied the dissolution of a substrate when acid particles are continuously injected at a single point and there is an external field that causes these particles to undergo biased diffusion. The basic quantities of interest in this process are the concentration profile of the acid and the growth kinetics of the dissolved region. Within the dissolved region, the acid concentration follows the steady-state profile of biased diffusion; this is just the solution of the anisotropic Laplace equation. The shape of the dissolved region is strongly anisotropic with its length growing in time as $\xi_{\|}\sim t^{2/(d+1)}$ while the transverse width grows as $\xi_{\perp}\sim t^{1/(d+1)}$.

A simple and relevant extension of our model is to the case of variable acid strength. This can be realized by assuming a substrate density $\rho>1$ so that ρ acid particles must hit a given substrate site before it dissolves (weak acid) or that an acid particle dissolves $A>1$ substrate sites before becoming neutralized (strong acid). In the current model, $\rho=A=1$. The case $A>1$ is equivalent to having a particle density in the substrate ρ equal to $1/A$ and with an acid particle dissolving one substrate particle. Incorporating this scaling behavior into Eq. (2) for the interface motion we have

$$\frac{\partial\vec{R}}{\partial t} = -\frac{D}{\rho}\vec{\nabla}c|_{|\vec{r}|=R(\theta,t)}. \tag{15}$$

For $\rho>1$, the dissolution boundary becomes smoother and grows more slowly since it takes many acid particles to dissolve each substrate site. For $d=1$, this follows immediately from the expression $v_I=\lambda v/(\lambda+\rho v)$ which was obtained from the flux balance argument (Sec. IV A). In general, Eqs. (1) and (2) are invariant after normalizing $c\to c/\rho$ and rescaling $\lambda\to\lambda/\rho$. This means that a change of the substrate density or acid strength will only change the time scale through the injection rate. We have tested this hypothesis by simulations in which acidity A varied between 1 and 160. At short times, the dissolution boundary appears to be much rougher for $\rho<1$. Asymptotically, it appears that the boundaries for different values of ρ approach a common limit. The overall effect of varying the acidity is simply to change the time scale. However, the subdominant terms to Eqs. (10) and (13) seem to have strong acidity dependence so that there is a long-lived transient correction to this simple scaling behavior (Fig. 6).

ACKNOWLEDGMENTS

We thank Paul Krapivsky for helpful discussions. We are also grateful to the ARO for Grant Nos. ARO DAAD19-99-1-0173 and the NSF for Grant No DMR9978902 for financial support.

[1] H. H. Uhlig, *Corrosion and Corrosion Control* (Wiley, New York, 1963).
[2] G. Daccord, Phys. Rev. Lett. **58**, 479 (1987).
[3] M. Sahimi, G.R. Gavalas, and T.T. Tsotsis, Chem. Eng. Sci. **45**, 1443 (1990).
[4] H.F. Meng and E.G.D. Cohen, Phys. Rev. E **51**, 3417 (1995).
[5] K.S. Kim, J.A. Hurtado, and H. Tan, Phys. Rev. Lett. **83**, 3872 (1999).
[6] A. Gabrielli, A. Baldassarri, and B. Sapoval, Phys. Rev. E **62**, 3103 (2000).
[7] H.S. Carslaw and J.C. Jaeger, *Conduction of Heat in Solids* (Oxford University Press, New York, 1959).
[8] J. Crank, *Free and Moving Boundary Value Problems* (Oxford University Press, New York, 1987).
[9] L.M. Cummings, Y. Hohlov, S.D. Howinson, and K. Kornev, J. Fluid Mech. **378**, 1 (1999).
[10] H. Larralde, Y. Lereah, P. Trunfio, J. Dror, S. Havlin, R. Rosenbaum, and H.E. Stanley, Phys. Rev. Lett. **70**, 1461 (1993).
[11] This is a simple exercise in extreme value statistics. For a general introduction see, e.g., J. Galambos, *The Asymptotic Theory of Extreme Order Statistics* (Krieger, Malabar, FL, 1987); for a discussion of the location of the extreme particle in diffusion, see S. Redner and P.L. Krapivsky, Am. J. Phys. **67**, 1277 (1999).
[12] S. Redner, *A Guide to First Passage Processes* (Cambridge University Press, New York, 2001).
[13] I.S. Gradstein and I.M. Rhzhik, *Table of Integrals, Series, and Products* (Academic Press, New York, 1967).
[14] *Handbook of Mathematical Functions*, edited by M. Abramowitz and I.A. Stegun (Dover, New York, 1965).
[15] W. Hwang and S. Redner, Phys. Rev. E **63**, 021508 (2001).
[16] E. Ben-Naim and S. Redner, J. Phys. A **25**, L575 (1992).